J Intell Robot Syst
DOI 10.1007/s10846-014-0170-2

# Attitude Estimation in SO(3): A Comparative UAV Case Study

**Alexandra Moutinho · Miguel Figueirôa · José Raul Azinheira**

Received: 25 August 2014 / Accepted: 18 November 2014


**Abstract** This paper introduces a novel algorithm to obtain attitude estimations from low cost inertial measurement units including 3-axis accelerometer, 3-axis gyroscope and 3-axis magnetometer. This nonlinear attitude estimator is derived from Lyapunov's theory and formulated in the special orthogonal group SO(3). The impact of the gyroscope bias is also assessed and an online estimator provided. The performance of the proposed estimator is validated and compared to current commonly used methods, namely the classical extended Kalman filter and two other nonlinear estimators in SO(3). Realistic simulations consider a quadcopter unmanned aerial vehicle subject to wind disturbances and whose sensors parameters have been identified from flight tests data.

This work was supported by Fundação para a Ciência e a Tecnologia (FCT), through IDMEC, under LAETA PEst-OE/EME/LA0022.

A. Moutinho (✉) · J. R. Azinheira
LAETA, IDMEC, Instituto Superior Técnico, Universidade de Lisboa, Av. Rovisco Pais, Pav. Mecânica 3, 1049-001 Lisbon, Portugal
e-mail: alexandra.moutinho@tecnico.ulisboa.pt

J. R. Azinheira
e-mail: jraz@dem.ist.utl.pt

M. Figueirôa
Instituto Superior Técnico, Universidade de Lisboa, Av. Rovisco Pais, 1049-001 Lisbon, Portugal
e-mail: miguel.figueiroa@tecnico.ulisboa.pt

**Keywords** Attitude estimation · Nonlinear observer · UAV · Online bias estimation · Inertial measurement unit

## 1 Introduction

The field of autonomous robots is fast expanding with applications ranging from commercial, military and scientific to disaster relief. Much of this growth stems from the recent availability of low cost sensors such as accelerometers and gyroscopes built from Micro-Electro-Mechanical Systems (MEMS). There have also been significant developments in attitude estimation algorithms, as the correct information of the attitude is key for the operation of most autonomous robotic platforms such as a bipedal humanoid robot, a sub-marine for oceanographic surveys, a surveillance airship or even a multirotor platform used for doorstep delivery of small but high value items such as electronic gadgets or urgent medicine.

Several methods have been proposed for attitude estimation using various methods. Some use the quaternion representation of rotation [5, 10, 17, 18, 22, 23] with measurements usually combined using variants of the Kalman filter [5, 10, 18, 22, 23]. Other authors use the rotation matrix formulation, benefiting from the associated Lie algebra properties [9, 13–15]. Attitude estimation can also be performed directly on the Euler angle formulations using complementary filtering techniques [24, 27]. Additionally the filter can

be formulated directly on the rotation representation using vectorial measurements [1].

Although it is possible to obtain an attitude estimate from an inertial measurement unit (IMU) comprised of 3-axis gyroscope, 3-axis accelerometer and 3-axis magnetometer, it is common to use additional sensors to improve the accuracy and/or measure information complementary to the measured states. Such is the case of vision-aided estimation using onboard cameras, either fish-eye [21], perspective [8] or even both [3]. Shabayek et al. recently published a survey of vision aided estimation methods [21]. When outdoor, it is also possible to use complementary GPS information [9, 26], or other sensors such as Doppler and laser radar [25], whereas indoor solutions may include laser range finding capabilities coupled with simultaneous location and mapping (SLAM) algorithms [6]. Two relevant compilations of attitude estimations algorithms are [2] and more recently [12].

In this paper we set out to introduce a novel Lyapunov-based algorithm for attitude estimation using the rotation matrix formulation. We also consider the effect of gyroscopic bias and what improvement can be gained from an online estimation solution. We assess the performance of the new attitude estimator comparing it to the extended Kalman filter (EKF), a classical and widely adopted solution and here used as baseline, and two other commonly used SO(3) solutions. Realistic simulations consider a quadcopter unmanned aerial vehicle subject to wind disturbances and whose sensors parameters, including bias and motors induced noise, have been identified from experimental data.

After this introduction, Section 2 presents the mathematical framework used and the considered sensor measurements. Section 3 reviews the attitude estimation solutions that will be compared to the proposed algorithm described in Section 4. Section 5 presents the comparative simulation results and Section 6 concludes with some final remarks.

## 2 Problem Statement

This section introduces the mathematical framework used throughout this paper and the sensor measurements considered for the attitude estimation algorithms.

### 2.1 Mathematical Framework

Throughout the paper, $\bar{x}$ and $\hat{x}$ represent respectively the measurement and the estimation of variable $x$.

The special orthogonal group is denoted by

$$\mathrm{SO}(3) = \left\{ A \in \mathbb{R}^{3\times 3} | A^T A = I, \det(A) = 1 \right\} \tag{1}$$

and its Lie algebra is denoted by $\mathfrak{so}(3)$, the set of anti-symmetric matrices.

The *cross map* $[\cdot]_\times : \mathbb{R}^{3\times 3} \mapsto \mathfrak{so}(3)$ is a Lie algebra isomorphism, with

$$[x]_\times = \begin{bmatrix} 0 & -x_3 & x_2 \\ x_3 & 0 & -x_1 \\ -x_2 & x_1 & 0 \end{bmatrix} \tag{2}$$

so that $[x]_\times y = x \times y, \forall_{x,y\in\mathbb{R}^3}$. The inverse of the cross map is denoted by the *vee map*, $[\cdot]_\vee : \mathfrak{so}(3) \mapsto \mathbb{R}^3$. The linear *trace map* $\mathrm{tr}(\cdot) : \mathbb{R}^{n\times n} \mapsto \mathbb{R}$ is defined by $\mathrm{tr}(A) = \{A \in \mathbb{R}^{n\times n} | \mathrm{tr}(A) = \sum_{i=1}^{n} a_{ii}\}$.

The following identities are used:

$$[x]_\times y = -[y]_\times x \tag{3}$$

$$[ax + by]_\times = a[x]_\times + b[y]_\times \tag{4}$$

$$\mathrm{tr}(A[x]_\times) = -x^T (A - A^T)_\vee \tag{5}$$

$$[Ax]_\times = A[x]_\times A^T \tag{6}$$

$$A^T[x]_\times + [x]_\times A = [(\mathrm{tr}(A)I - A)x]_\times \tag{7}$$

for $a, b \in \mathbb{R}$, $x, y \in \mathbb{R}^3$ and $A, I \in \mathbb{R}^{3\times 3}$.

The symmetric $\mathbb{P}_s(\cdot)$ and anti-symmetric $\mathbb{P}_a(\cdot)$ projection operators in the square matrix space are defined respectively as:

$$\mathbb{P}_s(A) = \frac{1}{2}(A + A^T), \quad \mathbb{P}_a(A) = \frac{1}{2}(A - A^T) \tag{8}$$

### 2.2 Measurements

A typical IMU can provide measurements from a 3-axis rate gyroscope, a 3-axis accelerometer and 3-axis magnetometer. The body reference frame, where the IMU is fixed, is denoted $\mathcal{B}$, whereas the fixed inertial reference frame is denoted $\mathcal{I}$. The rotation matrix $R$ corresponds to the transformation from $\mathcal{B}$ to $\mathcal{I}$.

#### *2.2.1 Rate Gyroscope*

The rate gyroscope measures the angular velocity of $\mathcal{B}$ relative to $\mathcal{I}$, expressed in $\mathcal{B}$. The error model used is

$$\bar{\omega} = \omega + \sigma_\omega + b_\omega \tag{9}$$

with $\omega \in \mathbb{R}^3$ denoting the true value of the angular rate, $\sigma_\omega$ denoting additive white noise and $b_\omega$ corresponding to a constant (or slowly time varying) bias term.

#### 2.2.2 Accelerometer

The accelerometer measures the instantaneous linear acceleration of $\mathcal{B}$ relative to $\mathcal{I}$ and expressed in $\mathcal{B}$, $a$, minus the effect of the gravitational acceleration expressed in $\mathcal{B}$:

$$\bar{a} = a - R^T \mathbb{g} + \sigma_a + b_a \tag{10}$$

where $\mathbb{g} \in \mathbb{R}^3$ is the constant gravitational acceleration vector. Again, the measurement $\bar{a}$ is corrupted by a white noise term $\sigma_a$ and a bias term $b_a$.

#### 2.2.3 Magnetometer

The magnetometer measures the specific Earth magnetic field vector, $\mathbb{m} \in \mathbb{R}^3$, expressed in $\mathcal{B}$:

$$\bar{n} = R^T \mathbb{m} + \sigma_n + d_n \tag{11}$$

The measurement $\bar{n}$ is disturbed not only by a usually low additive noise, $\sigma_n$, but also by local electromagnetic interferences $d_n$ due to, for instance, the electric motors of a mobile robot. For the purposes of estimation, in this paper we will not consider the local disturbances $d_n$ as it is customary in the literature [13, 15].

#### 2.2.4 Attitude from Vector Measurements

The rotation kinematics is described by

$$\dot{R} = R[\omega]_\times \tag{12}$$

The primary source of information regarding attitude are the rate gyros, but these suffer from the inconvenience of measuring the rate of change of $R$ as opposed to $R$ itself.

Both the magnetometer and the accelerometer provide vector measurements, respectively the direction of the magnetic North and the direction of gravity (when the acceleration of $\mathcal{B}$ is negligible). Each of these measurements constrains two of the three degrees of freedom of $R$ and if these vectors are not collinear they can be used to obtain a measurement of $R$, $\bar{R}$.

In this work we compute $\bar{R}$ using the singular value decomposition solution to Wahba's problem, as described in [16], which minimizes the cost function

$$J(\bar{R}) = \frac{1}{2} \sum_{i=1}^{2} w_i (\mathcal{V}_{\mathcal{I}i} - \bar{R}\mathcal{V}_{\mathcal{B}i})^T (\mathcal{V}_{\mathcal{I}i} - \bar{R}\mathcal{V}_{\mathcal{B}i}) \tag{13}$$

where $\mathcal{V}_{\mathcal{B}i}$ are the normalized accelerometer and magnetometer measurements $(\bar{a}, \bar{n})$, $\mathcal{V}_{\mathcal{I}i}$ are the normalized gravity and magnetic field vectors $(\mathbb{g}, \mathbb{m})$, and $w_i \in \mathbb{R}$ are positive weights.

## 3 Comparative Approaches

This section shortly presents the attitude estimation methods which will be used to compare and assess the performance of the novel estimator in SO(3).

### 3.1 Extended Kalman Filter

The extended Kalman filter (EKF) will be used as a performance benchmark as it is a classical attitude estimation method. Also, it is closer to the direct cosine matrix (DCM) formulation used in the following nonlinear filters as opposed to the quaternion form used in the also common multiplicative extended Kalman filter (MEKF). The EKF approach used here considers the attitude kinematics given by

$$\dot{\Phi} = \Theta(\Phi)\omega = f(x, u) \tag{14}$$

with

$$\Theta(\Phi) = \begin{bmatrix} 1 & \mathrm{s}_\phi \mathrm{t}_\theta & \mathrm{c}_\phi \mathrm{t}_\theta \\ 0 & \mathrm{c}_\phi & -\mathrm{s}_\phi \\ 0 & \mathrm{s}_\phi / \mathrm{c}_\theta & \mathrm{c}_\phi / \mathrm{c}_\theta \end{bmatrix} \tag{15}$$

where the short notations $\mathrm{s}_{(\cdot)} = \sin(\cdot)$, $\mathrm{c}_{(\cdot)} = \cos(\cdot)$ and $\mathrm{t}_{(\cdot)} = \tan(\cdot)$ were used. The rate gyros measurements are the observer input, $u = \bar{\omega}$. The observer estimates the attitude Euler angles $\Phi = [\phi, \theta, \psi]^T$ (corresponding to the estimator state $x$), that is later corrected by the measurements of the accelerometer and the magnetometer via the Kalman gain. This algorithm considers only the linearization around the yaw angle $\psi$, and therefore assumes small ($< 20°$) roll ($\phi$) and pitch ($\theta$) angles [7].

The observations are related with the state by

$$y = \left[\frac{\bar{a}_1}{\|\bar{a}\|}, \frac{\bar{a}_2}{\|\bar{a}\|}, \frac{\bar{n}_1}{\|\bar{n}_{12}\|}, \frac{\bar{n}_2}{\|\bar{n}_{12}\|}\right]^T = [-\theta, \phi, \cos\psi, \sin\psi]^T = h(x) \quad (16)$$

where the indices 1, 2 refer to the respective component of the measurement vector, $\bar{n}_{12} = [\bar{n}_1, \bar{n}_2]^T$, and $\|\cdot\|$ corresponds to the Euclidean norm.

The prediction step for iteration $k$ corresponds to

$$\hat{x}_k^- = f(\hat{x}_{k-1}, u_{k-1}) = \hat{x}_{k-1} + T_s \Theta(\hat{x}_{k-1})\bar{\omega}_{k-1} \quad (17)$$

$$P_k^- = F_{k-1} P_{k-1} F_k^T + Q_{k-1} \quad (18)$$

where $T_s$ is the sampling time, $F_{k-1} = \partial f/\partial x|_{\hat{x}_{k-1}, u_{k-1}}$, $Q_{k-1}$ is the process noise covariance matrix, and $P_{k-1}$ is the covariance matrix obtained in the previous iteration.

The filtering step is given by

$$K_k = P_k^- H_k^T (H_k P_k^- H_k^T + R_k)^{-1} \quad (19)$$

$$\hat{x}_k = \hat{x}_k^- + K_k \left(y_k - y_k^0 - h(\hat{x}_k^-)\right) \quad (20)$$

$$P_k = (I_3 - K_k H_k) P_k^- \quad (21)$$

with $H_k = \partial h/\partial x|_{\hat{x}_k^-}$, $R_k$ the observations noise covariance matrix, $K_k$ the Kalman gain matrix, and $y_k^0 = [0, 0, \frac{\bar{n}_{1,k-1}}{\|\bar{n}_{12}\|}, \frac{\bar{n}_{2,k-1}}{\|\bar{n}_{12}\|}]^T$ the observations trim condition.

### 3.2 Passive Complementary Filter in SO(3)

Mahony et al. [13] present three nonlinear attitude estimators in SO(3), one of which is the passive complementary filter (PCF), where the estimator for the rotation matrix is in the form

$$\dot{\hat{R}} = \hat{R}([\bar{\omega}]_\times + k_p \mathbb{P}_a(\tilde{R})) \quad (22)$$

with $k_p$ a positive scalar gain, $\tilde{R} = \hat{R}^T \bar{R}$ the rotation matrix estimation error, $\hat{R}$ and $\bar{R}$ the estimation and measurement, respectively, of the rotation matrix $R$, and $\mathbb{P}_a(\cdot)$ the skew-symmetric operator defined in Eq. 8.

### 3.3 Explicit Complementary Filter in SO(3)

Mahony et al. [13] also present the explicit version of the complementary filter. Instead of relying on a measured rotation matrix, this formulation directly uses the measured accelerometer and magnetometer directions to correct the estimated attitude. This allows for different scalar weights to be given to the accelerometer and magnetometer measurements, $k_a$ and $k_n$ respectively.

The explicit complementary filter (ECF) in SO(3) is given by

$$\dot{\hat{R}} = \hat{R}\,[\bar{\omega} + \alpha]_\times \quad (23)$$

with

$$\alpha = k_a(\bar{a} \times \hat{a}) + k_n(\bar{n} \times \hat{n}) \quad (24)$$

where $\hat{a}$ and $\hat{n}$ correspond to the expected acceleration and magnetic field vector measurements calculated as

$$\hat{a} = -\hat{R}^T \mathbb{g}, \quad \hat{n} = \hat{R}^T \mathbb{n} \quad (25)$$

In this formulation it is possible to assign different weights to the magnetometer and accelerometer measurements, whereas in the passive complementary filter this can be done depending on the method chosen to calculate $\bar{R}$.

## 4 Trace-Based Filter in SO(3)

This section presents the formulation of a new Lyapunov SO(3) attitude estimator.

### 4.1 Formulation

Given attitude and angular velocity measurements $(\bar{R}, \bar{\omega})$ and corresponding estimates $(\hat{R}, \hat{\omega})$, we consider an attitude error function $\Psi : \mathfrak{so}(3) \times \mathfrak{so}(3) \mapsto \mathbb{R}$, an attitude error vector $e_R \in \mathbb{R}^3$, and an angular velocity error vector $e_\omega \in \mathbb{R}^3$ as in [4]:

$$\Psi(\bar{R}, \hat{R}) = \frac{1}{2} \operatorname{tr}\left(D(I - \bar{R}^T \hat{R})\right) \quad (26)$$

$$e_R = \frac{1}{2}\left[D\bar{R}^T\hat{R} - \hat{R}^T\bar{R}D\right]_\vee \quad (27)$$

$$e_\omega = \hat{\omega} - \hat{R}^T\bar{R}\bar{\omega} \quad (28)$$

where $D \in \mathbb{R}^{3\times3}$ corresponds to a positive definite diagonal weighing matrix and $\Psi(\bar{R}, \hat{R})$ is locally positive-definite about $\hat{R} = \bar{R}$.

The definition of the angular velocity error vector $e_\omega$ is motivated by the comparison between $\dot{\hat{R}} \in \mathsf{T}_{\hat{R}}\mathrm{SO}(3)$ and $\dot{\bar{R}} \in \mathsf{T}_{\bar{R}}\mathrm{SO}(3)$ [11]. However, since they lie in different tangent spaces, they cannot be

directly compared. Comparing $\dot{\hat{R}}$ with the transformed $\dot{\bar{R}} \in \mathsf{T}_{\hat{R}}\mathrm{SO}(3)$ we obtain

$$\begin{aligned}\dot{\hat{R}} - \dot{\bar{R}}(\bar{R}^T\hat{R}) &= \hat{R}\left([\hat{\omega}]_\times - \hat{R}^T\bar{R}[\bar{\omega}]_\times\bar{R}^T\hat{R}\right)\\ &= \hat{R}[e_\omega]_\times \end{aligned} \tag{29}$$

To obtain the proposed attitude estimator, consider the following Lyapunov function candidate

$$W = a\Psi(\bar{R}, \hat{R}) + \frac{1}{2}e_\omega^T e_\omega \tag{30}$$

with $a$ a positive scalar parameter, and where $W > 0$ for $\hat{R} \to \bar{R}$, for any $\hat{R}, \bar{R} \in \mathrm{SO}(3)$. The time derivative of the Lyapunov function $W$ is given by

$$\begin{aligned}\dot{W} &= a\dot{\Psi}(\bar{R}, \hat{R}) + e_\omega^T\dot{e}_\omega\\ &= \frac{a}{2}\frac{\mathrm{d}}{\mathrm{dt}}\left(\mathrm{tr}\left(D(I - \bar{R}^T\hat{R})\right)\right) + e_\omega^T\dot{e}_\omega \end{aligned} \tag{31}$$

Let us look at the first parcel of Eq. 31. Knowing that the trace is a linear operator and hence commutes with the derivative, $\mathrm{d}\,\mathrm{tr}(x) = \mathrm{tr}(\mathrm{d}\,x)$, we have

$$\begin{aligned}\frac{a}{2}\frac{\mathrm{d}}{\mathrm{dt}}\left(\mathrm{tr}\left(D(I - \bar{R}^T\hat{R})\right)\right) &= -\frac{a}{2}\,\mathrm{tr}\left(D\frac{\mathrm{d}}{\mathrm{dt}}(\bar{R}^T\hat{R})\right)\\ &= -\frac{a}{2}\,\mathrm{tr}\left(D\bar{R}^T\hat{R}[e_\omega]_\times\right) \quad (32)\\ &= ae_\omega^T e_R \quad (33)\end{aligned}$$

where Eqs. 12, 6, 3 and 28 were sequentially used to obtain Eq. 32 and where Eqs. 5 and 27 were sequentially used to obtain Eq. 33.

The time derivative of the Lyapunov function $W$ is hence given by

$$\dot{W} = ae_\omega^T e_R + e_\omega^T\dot{e}_\omega = e_\omega^T(ae_R + \dot{e}_\omega) \tag{34}$$

If we choose the input $\dot{e}_\omega$ such that

$$ae_R + \dot{e}_\omega = -\Delta e_\omega \tag{35}$$

with $\Delta$ a positive definite diagonal weighing matrix, we guarantee that $\dot{W} < 0$ and the attitude estimator is (almost) globally asymptotically stable.

For known attitude and angular velocity measurements, $\bar{R}$ and $\bar{\omega}$, the estimator dynamics is then given by

$$\dot{e}_\omega = -\Delta e_\omega - ae_R \tag{36}$$

$$\dot{\hat{R}} = \hat{R}[\hat{\omega}]_\times \tag{37}$$

with

$$\hat{\omega} = e_\omega + \hat{R}^T\bar{R}\bar{\omega} \tag{38}$$

### 4.2 Discrete Implementation

For a sampling time $T_s$, the discrete implementation of the proposed estimator (36–37) is

$$e_{\omega,k+1} = e_{\omega,k} - T_s(\Delta e_{\omega,k} + ae_{R,k}) \tag{39}$$

$$\hat{R}_{k+1} = \hat{R}_k e^{T_s[\hat{\omega}_k]_\times} \tag{40}$$

where the matrix exponential $e^{T_s[\hat{\omega}_k]_\times}$ is calculated via the Rodrigues formula [20]

$$e^{T_s[\hat{\omega}_k]_\times} = I + \frac{\sin\vartheta}{\vartheta}[\hat{\omega}_k]_\times + \frac{\cos\vartheta - 1}{\vartheta^2}[\hat{\omega}_k]_\times^2 \tag{41}$$

with $\vartheta = T_s^2\sum_{i=1}^3\hat{\omega}_{i,k}^2$. The angular velocity estimation $\hat{\omega}_k$ is obtained from

$$\hat{\omega}_k = e_{\omega,k} + \hat{R}_k^T\bar{R}_k\bar{\omega}_k \tag{42}$$

Equations 39 and 42 can be condensed, resulting in the following discrete implementation of the proposed trace-based filter (TBF):

$$\hat{R}_{k+1} = \hat{R}_k e^{T_s[\hat{\omega}_k]_\times} \tag{43}$$

$$\begin{aligned}\hat{\omega}_{k+1} = {} & (1 - T_s\Delta)(\hat{\omega}_k - \hat{R}_k^T\bar{R}_k\bar{\omega}_k) - T_s ae_{R,k}\\ & + \hat{R}_{k+1}^T\bar{R}_{k+1}\bar{\omega}_{k+1}\end{aligned} \tag{44}$$

The form presented in Eq. 44 is useful to understand the effect of the design parameters:

- The positive definite diagonal matrix $\Delta$ defines the influence of the previous angular velocity estimation to the current one;
- The scalar gain $a$ determines the influence of the vectorial measurements in $e_R$;
- The positive definite matrix $D$ used in Eq. 27 to calculate $e_R$ sets the importance of the attitude correction provided by the measured attitude matrix $\bar{R}$ on roll, pitch and yaw individually.

### 4.3 Gyroscope Bias Estimation

A common limitation of current low cost gyroscopes is the presence of a small, slowly varying bias term, $b_\omega$. This bias term can significantly limit the usefulness of the gyroscope for determining the attitude. For this reason, many current attitude estimators also estimate the gyroscope bias term.

For any nonlinear estimator such as the ones in SO(3) from Section 3, the estimator dynamics is

$$\dot{\hat{R}} = \hat{R}[\hat{\omega}]_\times \tag{45}$$

where the calculation of estimated rotation velocity, $\hat{\omega}$, depends on the algorithm used.

In both nonlinear complementary algorithms, PCF and ECF, the estimated angular velocity $\hat{\omega}$ can be written as

$$\hat{\omega} = \bar{\omega} + \alpha \tag{46}$$

where $\alpha$ is a correction term based on the vectorial measurements, obtained via Eqs. 22 and 23 for the PCF and ECF, respectively. It is this correction term $\alpha$ that drives the bias estimation

$$\dot{\hat{R}} = \hat{R}[\bar{\omega} + \alpha - \hat{b}_\omega]_\times, \quad \dot{\hat{b}}_\omega = -k_{b_\omega}\alpha \tag{47}$$

where $0 < k_{b_\omega} < 1$ to capture only the low frequency aspect of the correction term $\alpha$. This modification maintains the original ECF and PCF stability proprieties [13].

To include the gyroscope bias estimation in the TBF, inspiration was drew from the nonlinear complementary filter bias formulation, and the fact that the TBF takes into consideration the existence of a rotation from the frame of $\hat{\omega}$ to the frame of $\bar{\omega}$, as in (29). We therefore redefine the correction term $\alpha$ as

$$\alpha = \hat{\omega} - \hat{R}^T \bar{R}\bar{\omega} + \hat{b}_\omega \tag{48}$$

which can also be written as

$$\alpha = e_\omega + \hat{b}_\omega \tag{49}$$

and therefore

$$\dot{\hat{b}}_\omega = -k_{b_\omega}(e_\omega + \hat{b}_\omega) \tag{50}$$

This formulation, where the bias estimation is derived from the angular velocity error, $e_\omega$, presents good simulation results, as shown in the next section.

## 5 Simulation Results

The four filters described in Sections 3 and 4 were used in simulation environment to estimate the attitude of a quadcopter UAV. Each estimator was evaluated at $50Hz$ with measurements from simulated sensors whose properties specified in Table 1 were identified from experimental data. Additionally, selected simulations also feature a gyroscope bias of $1°/s$ on all three axes.

Three missions with horizontal trajectories were considered (see Fig. 1):

- Mission 1, a $100m \times 100m$ square trajectory;
- Mission 2, a $300m \times 100m$ oval trajectory;
- Mission 3, a trajectory with three loops of $50m$ radius.

Missions 1 and 2 have a prescribed horizontal velocity of 5 $m/s$ while mission 3 features 10 $m/s$. The yaw angle is held constant at 10°.

Path following is accomplished via LQR control coupled with a PD controller for attitude and altitude stabilization. Simulations consider the presence of wind composed of a constant term $(2, 3, 0)$ $m/s$ added with 4 $m/s$ gusts from a Dryden Wind Turbulence model [19].

Initially the parameters for the extended Kalman filter (EKF) were derived directly from the sensor characteristics: the process noise covariance matrix $Q$ defined from the gyroscopic noise variance $\sigma_\omega^2$ and the measurement noise covariance matrix $R$ determined from the accelerometer and magnetometer noise characteristics, $\sigma_a$ and $\sigma_n$. However, some manual iteration suggested that better performance could be obtained using $Q_c = \text{diag}(\sigma_{\omega,1}^2, \sigma_{\omega,2}^2, \sigma_{\omega,3}^2)$ and $R_c = \text{diag}(1.26, 1.26, 3.06, 3.06) \times 10^{-2}$, with appropriate SI units.

The parameters for the nonlinear estimators were also iterated until good performance was achieved. The explicit complementary filter (ECF) parameters were set to $k_a = 0.5$ and $k_n = 1$. The passive complementary filter was tuned to $k_p = 0.3$, whereas for the trace-based filter (TBF) the parameters were set to $a = 1$, $D = \text{diag}(25, 25, 25)$ and $\Delta = \text{diag}(45, 45, 45)$. As stated in Section 2.2.4, the measured rotation matrix $\bar{R}$ is calculated via the singular value decomposition algorithm with $w_1 = 1$ and $w_2 = 5$.

The following results show the comparison of the attitude estimation obtained from the four approaches, and assesses the effect of gyroscopic bias and what improvement can be gained from the online estimation. Three cases were considered:

**Table 1** Sensors specifications

| | Units | Noise ($1\sigma$) | Quantization |
|---|---|---|---|
| Accelerometer | $m/s^2$ | 0.1 | 0.01 |
| Gyroscope | $°/s$ | 1 | 0.001 |
| Magnetometer | normalized | 0.05 | 0.01 |

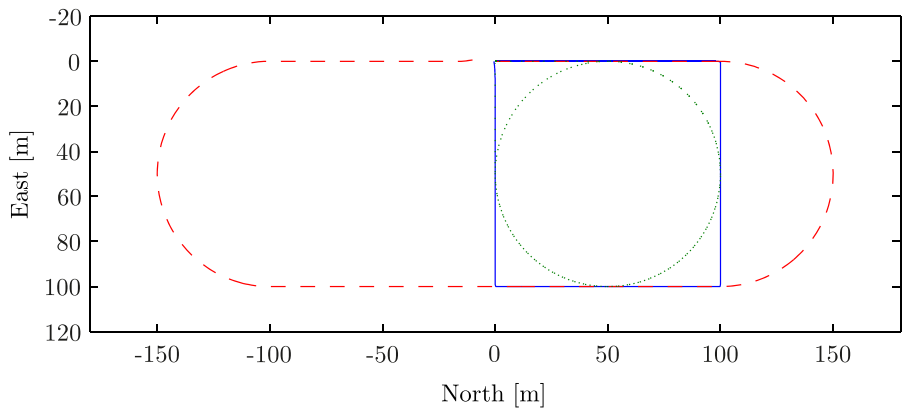


**Fig. 1** Reference trajectories of case-study missions (– Mission 1, – – Mission 2, : Mission 3)

**Table 2** Attitude estimation RMS errors for Case 1

| | Mission 1 | | | Mission 2 | | | Mission 3 | | |
|---|---|---|---|---|---|---|---|---|---|
| | $\phi$[°] | $\theta$[°] | $\psi$[°] | $\phi$[°] | $\theta$[°] | $\psi$[°] | $\phi$[°] | $\theta$[°] | $\psi$[°] |
| EKF | 1.51 | 1.05 | 3.99 | 1.08 | 1.31 | 3.07 | 3.65 | 3.32 | 6.49 |
| PCF | 1.98 | 0.50 | 2.74 | 1.19 | 0.41 | 1.65 | 5.11 | 1.25 | 7.29 |
| ECF | 1.80 | 1.03 | 1.94 | 1.05 | 0.66 | 1.33 | 4.23 | 1.80 | 5.03 |
| TBF | 2.11 | 0.61 | 3.45 | 1.23 | 0.37 | 1.82 | 5.34 | 1.28 | 8.33 |

**Table 3** Attitude estimation RMS errors for Case 2

| | Mission 1 | | | Mission 2 | | | Mission 3 | | |
|---|---|---|---|---|---|---|---|---|---|
| | $\phi$[°] | $\theta$[°] | $\psi$[°] | $\phi$[°] | $\theta$[°] | $\psi$[°] | $\phi$[°] | $\theta$[°] | $\psi$[°] |
| EKF | 6.56 | 6.42 | 12.58 | 6.48 | 6.55 | 12.32 | 7.30 | 7.00 | 13.04 |
| PCF | 3.93 | 3.23 | 4.32 | 3.70 | 3.22 | 3.79 | 5.89 | 3.39 | 8.42 |
| ECF | 4.28 | 1.10 | 7.94 | 4.11 | 0.73 | 8.02 | 5.56 | 1.69 | 8.68 |
| TBF | 3.59 | 3.05 | 4.13 | 3.26 | 2.93 | 2.66 | 5.88 | 3.32 | 9.08 |

**Table 4** Attitude estimation RMS errors for Case 3

| | Mission 1 | | | Mission 2 | | | Mission 3 | | |
|---|---|---|---|---|---|---|---|---|---|
| | $\phi$[°] | $\theta$[°] | $\psi$[°] | $\phi$[°] | $\theta$[°] | $\psi$[°] | $\phi$[°] | $\theta$[°] | $\psi$[°] |
| EKF | 2.69 | 1.89 | 6.28 | 2.06 | 2.04 | 4.75 | 5.58 | 5.02 | 10.25 |
| PCF | 2.49 | 0.92 | 3.39 | 1.62 | 0.73 | 2.18 | 6.73 | 1.99 | 9.60 |
| ECF | 2.35 | 1.14 | 3.49 | 1.56 | 0.72 | 2.60 | 5.48 | 1.76 | 8.32 |
| TBF | 2.64 | 0.98 | 3.88 | 1.60 | 0.69 | 2.08 | 6.85 | 1.94 | 9.53 |

– Case 1, with unbiased gyroscope measurements and the standard estimator formulation, i.e. without bias estimation;
– Case 2, with biased gyroscope measurements and the standard estimator formulation;
– Case 3, with biased gyroscope measurements and online bias estimation (see Section 4.3).

For the ECF and the PCF, the bias gain $k_{b_\omega}$ was set to 0.1, whereas for the TBF the bias estimation was achieved using Eq. 50 with a gain of $k_{b_\omega} = 0.1$. Each tuple (case, mission, estimator) was evaluated 30 times. Tables 2–4 summarize the estimation RMS errors for each of the three cases considered.

Case 1 is useful to evaluate the influence of the aggressiveness of the missions on the estimators. It can be seen that the higher aggressiveness of the third mission severely hampers the performance of all estimators, particularly the EKF. Case 1 also reveals the common tendency that the yaw angle ($\psi$) estimation is consistently less accurate that the pitch ($\theta$) and roll ($\phi$) angles, even more so in the case of the EKF and the

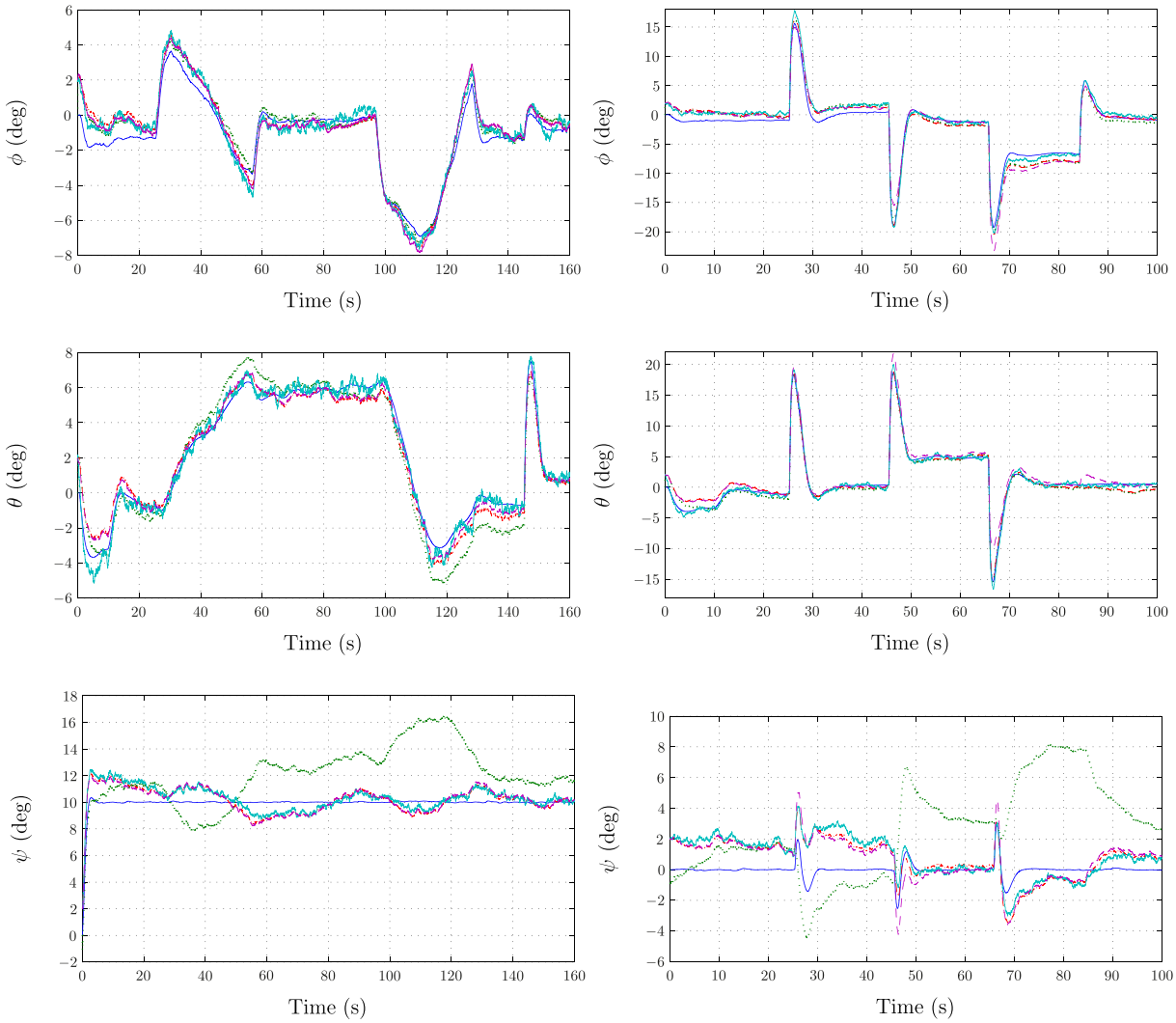


**Fig. 2** Performance of estimators for Mission 1 (*left*) and Mission 2 (*right*) (– true, : EKF –.– PCF, – – ECF, – TBF)

**Table 5** Angle RMSE results for Case 1 scenario

| | | Angle RMSE [°] | | |
|---|---|---|---|---|
| | | Roll | Pitch | Yaw |
| Mission 1 | EKF | 0.57 | 1.04 | 2.96 |
| | PCF | 0.71 | 0.81 | 0.90 |
| | ECF | 0.67 | 0.42 | 0.89 |
| | TBF | 0.65 | 0.71 | 0.86 |
| Mission 2 | EKF | 1.20 | 0.64 | 3.97 |
| | PCF | 1.18 | 0.68 | 1.40 |
| | ECF | 1.09 | 0.43 | 1.53 |
| | TBF | 1.34 | 1.10 | 1.35 |

PCF. This is most likely due to the higher noise of the magnetometer when compared to the accelerometer. Still for Case 1, one can see that the TBF and the ECF filters share the best performance, particularly for the roll and pitch angles.

As bias is added to the gyroscope, the accuracy of the estimators worsens significantly, as the correcting effect of the vectorial measurements cannot fully cancel the bias error. However, by adding the online estimation of the bias effect in Case 3, the performance is improved to figures closer to the ones of Case 1 for Missions 1 and 2 but not for Mission 3.

The performance of the estimators deteriorates as mission aggressiveness increases. Mission 2, the one with the smoothest trajectory, has about 1° RMSE for each angle. Mission 1 has 2° RMSE, rising for 3° RMSE for Mission 3, the one with the most aggressive maneuvers.

The left and right graphics in Fig. 2 compare the attitude estimation results obtained using the four approaches with their true values for Missions 1 and 2 for Case 1 scenario. Table 5 shows the estimators attitude root mean square (RMS) errors for both missions.

It can be seen from the simulation results in Fig. 2 and in Table 5 that the EKF provides good estimates for the roll and pitch angles, with RMS errors below 1.2° for both missions. For Mission 2 one can also see that the EKF formulation is more sensitive to the coupling of the rotation axes, as the yaw estimates are severely influenced by changes in the pitch and roll angles.

For both missions, the three nonlinear approaches provide similar performances, with the ECF providing the best overall accuracy.

All estimators performed better for Mission 1, as it consists of a smoother trajectory and thus fewer disturbances to measure the gravity vector, $\bar{a}$ in (10). It is interesting to compare the PCF with the TBF presented in this work, as they both rely on a measured attitude matrix $\bar{R}$. The performance is similar, with the TBF performing slightly worse in the estimation of roll and pitch for Mission 2, but slightly better for Mission 1. Regarding the estimation of yaw, the proposed TBF shows the best results for both missions.

## 6 Conclusions

A novel nonlinear algorithm for attitude estimation in SO(3) was formulated according to Lyapunov theory, thus guaranteeing the (almost) asymptotic convergence of the estimation error.

The proposed estimator performance was compared in simulation with the extended Kalman filter and two other commonly used nonlinear solutions in SO(3) proposed in the current literature, the passive and explicit complementary filters. Despite featuring reasonable performance in the roll and pitch axes, the studied extended Kalman filter formulation provides poor yaw angle estimates. Sharing similar accuracy, all the studied attitude estimator formulations in SO(3) outperform the extended Kalman filter and present a good approach provided the vehicle is restricted to smooth trajectories, that is, acceleration is kept within a small bound. The proposed trace-based filter method for gyroscope bias estimation leads to good performance, at times outperforming both the passive and explicit complementary filters results. Uncompensated gyroscope bias can have significant detrimental effects on attitude estimation, regardless of the estimation method used.

Future work includes i) the evaluation of the effect of changing the weights in the singular value decomposition solution to Wahba's problem, and ii) the experimental validation of the proposed filter with a comparison of the computational effort of the different attitude estimators.

## References


1. Batista, P., Silvestre, C., Oliveira, P.: Sensor-based globally asymptotically stable filters for attitude estimation: Analysis, design, and performance evaluation. IEEE Trans. Autom. Control **57**(8), 2095–2100 (2012)
2. Crassidis, J., Markley, F., Chen, Y.: Survey of nonlinear attitude estimation methods. J. Guid., Control Dyn. **30**(1), 12–28 (2007)
3. Eynard, D., Vasseur, P., Demonceaux, C., Frémont, V.: UAV altitude estimation by mixed stereoscopic vision. In: Proceedings IEEE/RSJ International Conference on Intelligent Robots and Systems, pp. 646–651. IEEE, Taipei (2010)
4. Fernando, T., Chandiramani, J., Lee, T., Gutierrez, H.: Robust adaptive geometric tracking controls on SO(3) with an application to the attitude dynamics of a quadrotor UAV. In: Proceedings 50th IEEE Conference on Decision and Control and European Control Conference, pp. 7380–7385. IEEE, Orlando (2011)
5. Gebre-Egziabher, D., Elkaim, G.H., Powell, J.D., Parkinson, B.W.: A gyro-free quaternion-based attitude determination system suitable for implementation using low cost sensors. In: Proceedings Position Location and Navigation Symposium, pp. 185–192. IEEE (2000)
6. Grzonka, S., Grisetti, G., Burgard, W.: A fully autonomous indoor quadrotor. IEEE Trans. Robot. **28**(1), 90–100 (2012)
7. Henriques, B.: Estimation and control of a quadrotor attitude. Master thesis, Instituto Superior Tecnico, Universidade Tecnica de Lisboa (2011)
8. Honegger, D., Meier, L., Tanskanen, P., Pollefeys, M.: An open source and open hardware embedded metric optical flow CMOS camera for indoor and outdoor applications. In: Proceedings IEEE International Conference on Robotics and Automation, pp. 1736–1741. IEEE, Karlsruhe (2013)
9. Hua, M.D.: Attitude estimation for accelerated vehicles using GPS/INS measurements. Control. Eng. Pract. **18**(7), 723–732 (2010)
10. Kumar, N.S., Jann, T.: Estimation of attitudes from a low-cost miniaturized inertial platform using Kalman filter-based sensor fusion algorithm. Sadhana **29**(2), 217–235 (2004)
11. Lee, T.G., Leoky, M., McClamroch, N.H.: Geometric tracking control of a quadrotor UAV on SE(3). In: Proceedings 49th IEEE Conference on Decision and Control, pp. 5420–5425. IEEE, Atlanta (2010)
12. Madinehi, N.: Rigid body attitude estimation: An overview and comparative study. Master thesis, Western University Canada (2013)
13. Mahony, R., Hamel, T., Pflimlin, J.M.J.: Nonlinear complementary filters on the special orthogonal group. IEEE Trans. Autom. Control **53**(5), 1203–1218 (2008)
14. Mahony, R., Hamel, T., Trumpf, J., Lageman, C.: Nonlinear attitude observers on SO(3) for complementary and compatible measurements: A theoretical study. In: Proceedings Joint 48th IEEE Conference on Decision and Control and 28th Chinese Control Conference, pp. 6407–6412. IEEE, Shanghai (2009)
15. Mahony, R., Kumar, V., Corke, P.: Multirotor aerial vehicles: Modeling, estimation, and control of quadrotor. IEEE Robot. Autom. Mag. **19**(3), 20–32 (2012)
16. Markley, F.: Attitude determination using vector observations and the singular value decomposition. J. Astronaut. Sci **36**(3), 245–258 (1988)
17. Markley, F.L., Mortari, D.: Quaternion attitude estimation using vector observations. J. Astronaut. Sci. **48**(2-3), 359–380 (2000)
18. Martin, P., Salaun, E.: Generalized multiplicative extended Kalman filter for aided attitude and heading reference system. In: Proceedings Guidance, Navigation and Control Conference, pp. 1–13. AIAA, Toronto (2010)
19. Mathworks: Dryden Wind Turbulence Model, Matlab Aerospace Toolbox (2014)
20. Politi, T.: A formula for the exponential of a real skew-symmetric matrix of order 4. BIT **41**(4), 842–845 (2001)
21. Shabayek, A.E.R., Demonceaux, C., Morel, O., Fofi, D.: Vision based UAV attitude estimation: Progress and insights. J. Intell. Robot. Syst. **65**(1-4), 295–308 (2012)
22. Shuster, M.D.: A simple Kalman filter and smoother for spacecraft attitude. J. Astronaut. Sci. **37**(1), 86–106 (1989)
23. Vandyke, M.C., Schwartz, J.L., Hall, C.D.: Unscented Kalman filtering for spacecraft attitude state and parameter estimation. In: Proceedings AAS/AIAA space flight mechanics conference (2004)
24. Vasconcelos, J. et al.: Discrete-time complementary filters for attitude and position estimation: Design, analysis and experimental validation. IEEE Trans. Control Syst. Technol. **19**(1), 181–198 (2011)
25. Vasconcelos, J.F., Cunha, R., Silvestre, C., Oliveira, P.: A nonlinear position and attitude observer on SE(3) using landmark measurements. Syst. Control Lett. **59**(3-4), 155–166 (2010)
26. Vasconcelos, J.F., Silvestre, C., Oliveira, P.: A nonlinear GPS/IMU based observer for rigid body attitude and position estimation. In: Proceedings 47th IEEE Conference on Decision and Control, pp. 1255–1260. IEEE, Cancun (2008)
27. Yoo, T., Hong, S., Yoon, H., Park, S.: Gain-scheduled complementary filter design for a MEMS based attitude and heading reference system. Sensors **11**(4), 3816–3830 (2011)